Laminar Flow in the Inlet Section of Parallel Plates

Y. L. WANG and P. A. LONGWELL

California Institute of Technology, Pasadena, California

Velocity distributions, pressure gradients, and overall pressure drops are presented. A definite concavity was found in the velocity profile near the entrance for case I. In case II, which is more realistic physically, very definite effects are transmitted upstream, and the velocity distributions downstream show little concavity.

The steady laminar flow of an incompressible Newtonian fluid in the inlet section of parallel plates has been investigated by several authors (*1, 2, 3, 4, 5*) using boundary-layer theory. In all cases the velocity distribution at the entrance was assumed to be flat, and the assumptions inherent in boundary-layer theory were made, that is both the derivative $\partial^2 u_x/\partial x^2$ and the pressure gradient normal to the plates were neglected. Schlichting (*1, 2*) integrated the boundary-layer equations downstream from the entrance and joined this solution with one obtained by integrating the same equations in the upstream direction from the asymptotic parabolic distribution. Bodoia and Osterle (*3*) numerically integrated the boundary-layer equations, and Collins and Schowalter (*4, 5*) used Schlichting's method with refinements.

Although boundary-layer theory is a powerful tool, it is well known that its assumptions are not valid in the vicinity of the leading edge of a plate such as is found in this case. In this region the derivative $\partial^2 u_x/\partial x^2$ is not negligible relative to $\partial^2 u_x/\partial y^2$, and the pressure gradients in the y direction are not necessarily small so that the momentum equation for u_y is not negligible. Likewise the assumption of a flat velocity distribution at the entrance is artificial, and it seems much more likely that the velocity distribution upstream of the entrance will show some effects of the plates.

A numerical solution is reported herein which does not use the boundary-layer assumptions and is therefore an exact solution in the sense that no terms in the momentum equations which are not identically zero have been neglected. Two cases were studied, the first with the assumption of a flat velocity distribution at the entrance and the second with a flat distribution far upstream of the entrance. Results for a Reynolds number of 300 are presented.

FORMULATION OF PROBLEM

The physical situation considered is for the isothermal laminar flow of an incompressible Newtonian fluid under steady state conditions. There is an infinite number of flat plates of negligible thickness and semi-infinite length, separated from one another by distances $2y_o$, and lying parallel to the $x - z$ plane between $x = 0$ and $x = \infty$. The velocity of the fluid at a large distance upstream from the entrance is equal to U, is parallel to the x axis, and is independent of y and z. At large distances downstream the velocity distribution between pairs of plates becomes parabolic, so the dimension of the problem is from $-\infty$ to $+\infty$ in the x direction.

The flow between the plates is independent of z, and the equations of continuity and motion are in dimensionless form

$$\frac{\partial u_x}{\partial x} + \frac{\partial u_y}{\partial y} = 0 \tag{1}$$

$$u_x \frac{\partial u_x}{\partial x} + u_y \frac{\partial u_x}{\partial y} = -\frac{\partial P}{\partial x} + \frac{4}{N_{Re}}\left(\frac{\partial^2 u_x}{\partial x^2} + \frac{\partial^2 u_x}{\partial y^2}\right) \tag{2}$$

$$u_x \frac{\partial u_y}{\partial x} + u_y \frac{\partial u_y}{\partial y} = -\frac{\partial P}{\partial y} + \frac{4}{N_{Re}}\left(\frac{\partial^2 u_y}{\partial x^2} + \frac{\partial^2 u_y}{\partial y^2}\right) \tag{3}$$

When one takes the $x - z$ plane to lie at the midplane between two parallel plates, it is only necessary to consider the flow between $y = 0$, at the center plane and $y = 1$ at the upper plate. The boundary conditions for the downstream section $x > 0$ are

$$u_x = u_y = 0 \text{ at } y = 1 \tag{4}$$

$$\frac{\partial u_x}{\partial y} = 0,\ u_y = 0 \text{ at } y = 0 \tag{5}$$

$$u_x = \frac{3}{2}(1 - y^2),\ u_y = 0 \text{ at } x = \infty \tag{6}$$

For case I the velocity distribution at the entrance is taken as flat, or

$$u_x = 1,\ u_y = 0 \text{ at } x = 0 \tag{7}$$

For case II the velocity distribution at the entrance is unknown, and the following boundary conditions are applied to the region $x < 0$:

$$\frac{\partial u_x}{\partial y} = 0,\ u_y = 0 \text{ at } y = 1 \text{ and at } y = 0 \tag{8}$$

$$u_x = 1,\ u_y = 0 \text{ at } x = -\infty \tag{9}$$

METHOD OF SOLUTION

The stream function ψ defined in the usual manner

$$u_x = \frac{\partial \psi}{\partial y}\ u_y = -\frac{\partial \psi}{\partial x} \tag{10}$$

is introduced, and the elimination of the pressure gradients from Equations (2) and (3) gives a single equation for ψ:

$$\frac{\partial \psi}{\partial y}\frac{\partial}{\partial x}(\nabla^2 \psi) - \frac{\partial \psi}{\partial x}\frac{\partial}{\partial y}(\nabla^2 \psi) = \frac{4}{N_{Re}}\nabla^4 \psi \tag{11}$$

Equation (11) can also be written as the vorticity transport equation

$$\frac{\partial \psi}{\partial y}\frac{\partial \omega}{\partial x} - \frac{\partial \psi}{\partial x}\frac{\partial \omega}{\partial y} = \frac{4}{N_{Re}}\nabla^2 \omega = \frac{4}{N_{Re}}\left(\frac{\partial^2 \omega}{\partial x^2} + \frac{\partial^2 \omega}{\partial y^2}\right) \tag{12}$$

with the vorticity defined as

Y. L. Wang is with the Burroughs Corporation, Pasadena, California.

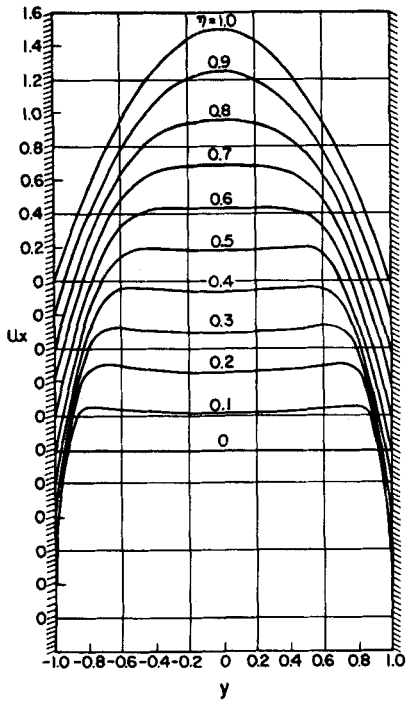

Fig. 1. Velocity profiles, case I.

$$\omega = \frac{\partial u_y}{\partial x} - \frac{\partial u_x}{\partial y} = -\nabla^2\psi = -\left(\frac{\partial^2\psi}{\partial x^2} + \frac{\partial^2\psi}{\partial y^2}\right) \quad (13)$$

The numerical treatment of a problem which has infinite boundaries is awkward, so a transformation from x to a new independent variable η is used to make the boundaries finite. Several forms were considered, and the form selected is

$$\eta = 1 - (1 + cx)^{-1} \quad (14)$$

in which c is a constant with a positive value for $x > 0$ and a negative value for $x < 0$. This transformation compresses the scale in terms of x at large distances from the entrance, where gradients are small, which is advantageous for a finite difference solution. Both the upstream and downstream regions are transformed into squares, $0 \leq y \leq 1$ and $0 \leq \eta \leq 1$.

The differential equations finally used are

$$\frac{d\eta}{dx}\left(\frac{\partial\psi}{\partial y}\frac{\partial\omega}{\partial\eta} - \frac{\partial\psi}{\partial\eta}\frac{\partial\omega}{\partial y}\right) = \frac{4}{N_{Re}}\left[\frac{d^2\eta}{dx^2}\frac{\partial\omega}{\partial\eta} + \left(\frac{d\eta}{dx}\right)^2\frac{\partial^2\omega}{\partial\eta^2} + \frac{\partial^2\omega}{\partial y^2}\right] \quad (15)$$

and

$$-\omega = \frac{d^2\eta}{dx^2}\frac{\partial\psi}{\partial\eta} + \left(\frac{d\eta}{dx}\right)^2\frac{\partial^2\psi}{\partial\eta^2} + \frac{\partial^2\psi}{\partial y^2} \quad (16)$$

Table 1. The $\eta - x$ Relation for $c = 1.2$

η	$\pm x$	η	$\pm x$
0	0	0.55	1.01852
0.05	0.04386	0.60	1.25000
0.10	0.09259	0.65	1.54762
0.15	0.14706	0.70	1.94444
0.20	0.20833	0.75	2.50000
0.25	0.27778	0.80	3.33333
0.30	0.35714	0.85	4.72222
0.35	0.44872	0.90	7.50000
0.40	0.55556	0.95	15.83333
0.45	0.68182	1.00	∞
0.50	0.83333		

The boundary conditions for the downstream region become

$$\psi = 1, \frac{\partial\psi}{\partial y} = 0 \text{ at } y = 1 \quad (17)$$

$$\psi = 0, \ \omega = 0 \text{ at } y = 0 \quad (18)$$

$$\psi = \frac{3}{2}y - \frac{1}{2}y^3, \ \omega = 3y \text{ at } \eta = 1 \quad (19)$$

These are straightforward except that ω is not known explicitly at $y = 1$.

For case I the boundary condition at the entrance is

$$\psi = y, \ \omega = 0 \text{ at } \eta = 0 \quad (20)$$

For case II the upstream region boundary conditions are

$$\psi = 1, \ \omega = 0 \text{ at } y = 1 \quad (21)$$

$$\psi = 0, \ \omega = 0 \text{ at } y = 0 \quad (22)$$

$$\psi = y, \ \omega = 0 \text{ at } \eta = 1 \quad (23)$$

The general scheme of solution used was to express the partial differential equations in finite difference form and to attempt to obtain a solution by iterative methods. Because of the nonlinearity of the problem this was by no means straightforward, and several formulations gave divergence except at very low Reynolds number. These trials are outlined in the Appendix. The scheme which was found to be convergent uses Equations (15) and (16) which involve both ψ and ω as functions of η and y. The finite difference equation for ω uses Allen's method (6) and is derived in the Appendix as Equation (A8). The finite difference equation for ψ is derived in the Appendix as Equation (A16).

The procedure for solving case II was more complicated than that for case I and will be described. The increments in η and y were chosen as equal, that is $a/b = 1$. Values of ψ and ω were assigned to the boundary points in accordance with the boundary conditions, and initial estimates of ω and ψ were made for the interior points, including those at $\eta = 0$.

In carrying out the iterative calculations the downstream region, the upstream region, and the line at $\eta = 0$ were treated separately. One complete iterative consisted of the following steps:

1. New ψ's were calculated at $\eta = 0$.
2. New ψ's were calculated for the downstream region.
3. New ψ's were calculated for the upstream region.
4. New ω's were calculated at $\eta = 0$.
5. New ω's were calculated for the downstream region.
6. New ω's were calculated for the upstream region.

Single step iteration was used; that is the latest values of ψ and ω were used in each calculation. It was found that the rate of convergence of the solution could be increased by a factor of 4 or so by the method of successive relaxation (7)* which is described in the Appendix. The relaxation factors M_ψ and M_ω were constant for an iteration but not necessarily equal. Values used varied from 1.5 to 0.5, and the choice was both empirical and somewhat arbitrary.

At the end of an iteration the degree of convergence defined as

$$\text{degree of convergence} = \max \frac{\psi_E^{(k+1/2)} - \psi_E^{(k)}}{\psi_E^{(k)}} \quad (24)$$

was used as a criterion to decide whether additional iterations were necessary. A criterion of 2×10^{-8} was used, which was the limit of the Burroughs-220 and IBM-7090 computers used.

When the solution was judged to have converged, the

* The term "relaxation" is used here rather than the conventional over relaxation, as both over and under relaxation are used.

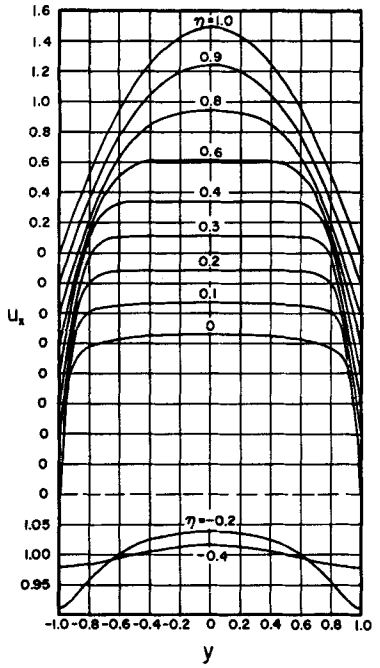

Fig. 2. Velocity profiles, case II.

point velocities were calculated from Equations (A20) and (A21), and pressure gradients were calculated from Equations (A23) and (A24).

Case I and case II were solved for a Reynolds number of 300 with $\Delta y = \Delta\eta = 0.05$. The constant c in Equation (14) was taken as 1.2 in both cases.

RESULTS

The calculations resulted in values of ψ, ω, u_x, u_y, $\partial P/\partial\eta$, $\partial P/\partial x$, and $\partial P/\partial y$ at each grid point with intervals of 0.05 in η and in y for both cases I and II at a Reynolds number of 300. These, as well as the results of preliminary calculations with $\Delta y = \Delta\eta = 0.10$, are reported (8). Abridged tables giving u_x, u_y, $\partial P/\partial x$, and $\partial P/\partial y$ for both cases are available (9).

The velocity profiles found for case I are shown in Figure 1. The values on the curves are the location in terms of η, and the values of x corresponding to these can be found in Table 1. It will be noted in Figure 1 that the velocity distribution is concave ($\partial^2 u_x/\partial y^2 > 0$) in the central portion for the first few values of η, and inspection of the numerical results reveals that this is true for η's as large as 0.6. This is in contradistinction to the results obtained by boundary-layer theory for which a flat distribution in the central region is assumed close to the entrance.

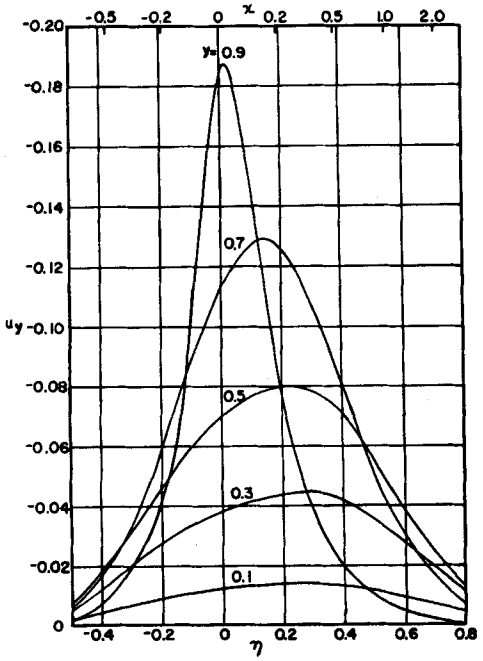

Fig. 3. u_y as function of η, case II.

Table 2. Comparison of Results for u_x

y	Schlichting's	Case I	Case II	Schlichting's	Case I	Case II
	η = 0 x = 0			η = 0.05 x = 0.043859		
0.95	1.0	1.0	0.7052	0.705	0.8281	0.8220
0.9	1.0	1.0	0.8862	1.007	0.9958	0.8753
0.8	1.0	1.0	0.9817	1.040	1.0324	1.0004
0.7	1.0	1.0	1.0143	1.040	1.0268	1.0280
0.6	1.0	1.0	1.0321	1.040	1.0214	1.0421
0.5	1.0	1.0	1.0439	1.040	1.0178	1.0514
0.4	1.0	1.0	1.0509	1.040	1.0155	1.0578
0.3	1.0	1.0	1.0560	1.040	1.0140	1.0622
0.2	1.0	1.0	1.0593	1.040	1.0131	1.0651
0.1	1.0	1.0	1.0612	1.040	1.0126	1.0667
0.0	1.0	1.0	1.0618	1.040	1.0124	1.0672
	η = 0.20 x = 0.208333			η = 0.50 x = 0.83333		
0.95	0.399	0.4261	0.4141	0.245	0.2166	0.2428
0.9	0.720	0.7624	0.7292	0.487	0.4247	0.4662
0.8	1.046	1.0815	1.0188	0.808	0.7877	0.8274
0.7	1.088	1.1046	1.0759	1.082	1.0303	1.0442
0.6	1.088	1.0940	1.0831	1.130	1.1483	1.1398
0.5	1.088	1.0807	1.0847	1.182	1.1889	1.1705
0.4	1.088	1.0713	1.0861	1.192	1.1967	1.1768
0.3	1.088	1.0650	1.0875	1.196	1.1946	1.1764
0.2	1.088	1.0610	1.0885	1.196	1.1912	1.1750
0.1	1.088	1.0588	1.0892	1.196	1.1888	1.1741
0.0	1.088	1.0581	1.0894	1.196	1.1880	1.1737
	η = 0.80 x = 3.33333			η = 0.90 x = 7.50000		
0.95	0.172	0.1712	0.1742	0.156	0.1542	0.1550
0.9	0.333	0.3315	0.3371	0.302	0.2998	0.3011
0.8	0.619	0.6177	0.6266	0.568	0.5644	0.5665
0.7	0.858	0.8547	0.8639	0.797	0.7929	0.7953
0.6	1.041	1.0390	1.0455	0.989	0.9847	0.9867
0.5	1.175	1.1715	1.1736	1.143	1.1398	1.1409
0.4	1.265	1.2587	1.2562	1.281	1.2598	1.2596
0.3	1.317	1.3111	1.3048	1.347	1.3474	1.3460
0.2	1.338	1.3397	1.3309	1.404	1.4063	1.4037
0.1	1.346	1.3533	1.3431	1.436	1.4400	1.4366
0.0	1.347	1.3572	1.3466	1.446	1.4509	1.4473

Velocity profiles for case II are shown in Figure 2 in which two upstream velocity profiles are included. It is seen that there is a noticeable effect upstream of the entrance and that the velocity distribution at the entrance $\eta = 0$ is smooth. Central concavity of the velocity distribution is not evident in Figure 2, although it is present to a small extent for values of η between 0.30 and 0.60 and is most pronounced at $\eta = 0.40$, where the maximum velocity is 0.5% higher than that at the center. It is judged that this concavity is a real effect as it is present to a similar extent in the preliminary solution found with coarser grid (8).

The velocity profiles for case I and case II are compared with those of Schlichting at selected locations in Table 2. As would be expected they agree well at large x and are most different close to entrance. In fact if the inlet length is defined as the distance from the entrance at which the center-line velocity reaches 98% of its asymptotic value, it is found that inlet lengths are quite insensitive to the calculation method. In terms of the dimensionless quantity $\nu x'/2y_o^2 U = 2x/N_{Re}$ the value for case I is 0.067, that for case II is 0.068, and others (3, 4, 5) report values in the range 0.068 to 0.069.

A comparison of velocities at the center line with those

Table 3. Comparison of Center-line Velocities with Those of Collins and Schowalter

		Center-line velocities			
x	η	Case I*	Case II*	C. & S.†	Ref.
1.19	0.588	1.231	1.212	1.200	4
2.588	0.756	1.324	1.311	1.28	5
5.175	0.861	1.413	1.407	1.40	5

* By linear interpolation with respect to η in reference 8.
† Collins and Schowalter.

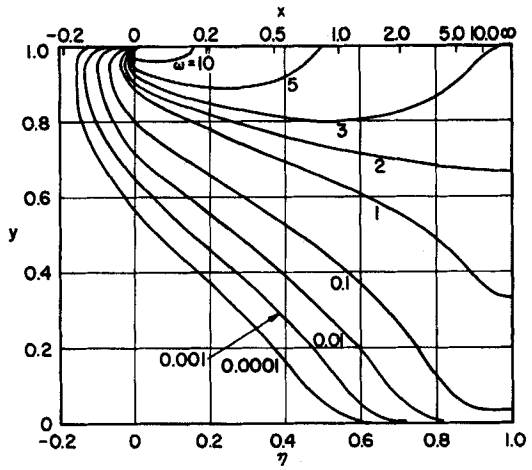

Fig. 4. Lines of constant vorticity, case II.

obtained by Collins and Schowalter (*4, 5*) is given in Table 3. Their values are a little smaller than those calculated by the authors; however the velocity distributions are similar in shape in the region for which data are reported (*4, 5*). Unfortunately Collins and Schowalter did not show distributions close to the entrance.

The velocity components in the y direction are quite significant near the entrance. These are shown for case II in Figure 3. The largest value found is -0.186 at $x = 0$, $y = 0.90$. As u_y is zero at $y = 1$, it is evident that the velocity gradient is high near the leading edge of the plate.

Figure 4 shows lines of constant vorticity for case II. The diffusion of vorticity from the plate can be visualized, and it is seen that the diffusion in the upstream direction is significant near the leading edge.

As would be expected the pressure gradients are largest in the vicinity of the leading edge of the plate. Figure 5 shows $-\partial P/\partial x$ as a function of η in this vicinity. The leading edge is a discontinuity, and the numerical results at $y = 1$ and 0.95 can only be considered as semiquantitative; a finer grid spacing in the immediate vicinity of the leading edge would give better results. For clarity $-\partial P/\partial x$ is shown for smaller values of y in Figure 6. The value of

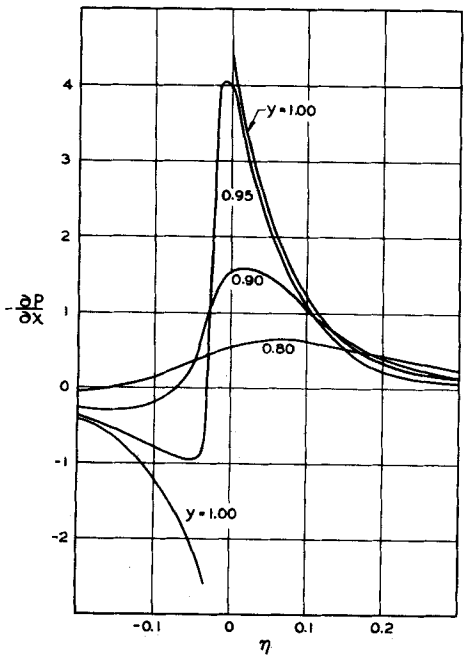

Fig. 5. $\partial P/\partial x$ close to leading edge, case II.

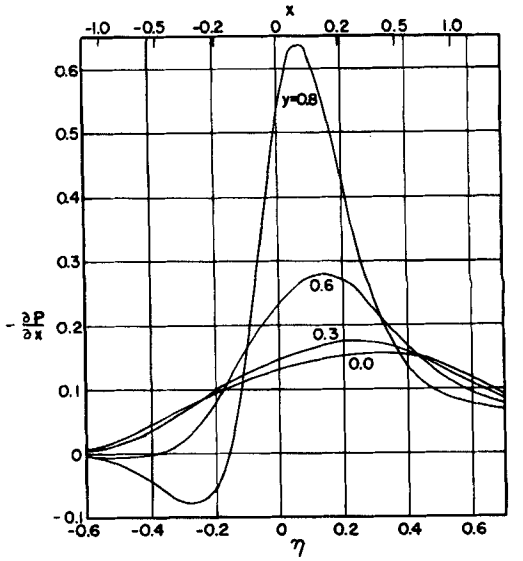

Fig. 6. $\partial P/\partial x$ as function of η, case II.

$-\partial P/\partial x$ for the fully developed parabolic profile at $x = \infty$ is 0.04 for a Reynolds number of 300.

Figure 7 shows $-\partial P/\partial y$ near the entrance. It is evident that this gradient is by no means negligible in this region.

Table 4 shows a comparison of pressure drops in the inlet region for case I, case II, and Schlichting's solution. Simpson's rule was used to evaluate $\int (\partial P/\partial \eta)\, d\eta$ for the first two. The quantity shown is equal to the pressure decrease with reference to free stream conditions minus that which would occur in the stated length for fully developed parabolic flow, which is $0.04x$ for this Reynolds number. The quantity shown can be considered as an entrance loss in terms of dimensionless pressure but includes that pressure drop due to the increase in kinetic energy; the latter amounts to 0.2714 for fully developed parabolic flow. Schlichting's solution neglects pressure gradients in the y direction, so only one value is shown for a given x, and this appears to be low. As the values of $\partial P/\partial y$ are very small at $\eta = 0.95$, no differences with y should be found at this location. However in case I the value for $y = 0.9$ is much smaller than for $y = 0.5$ or 0.1. This difference may be due in part to discretization error near the discontinuity at the entrance. However it is believed indicative that case I does not represent a real physical situation, since at $y = 0.9$ there is a reversal in pressure gradient $-\partial P/\partial x$ between $\eta = 0.3$ and 0.45, and this is re-

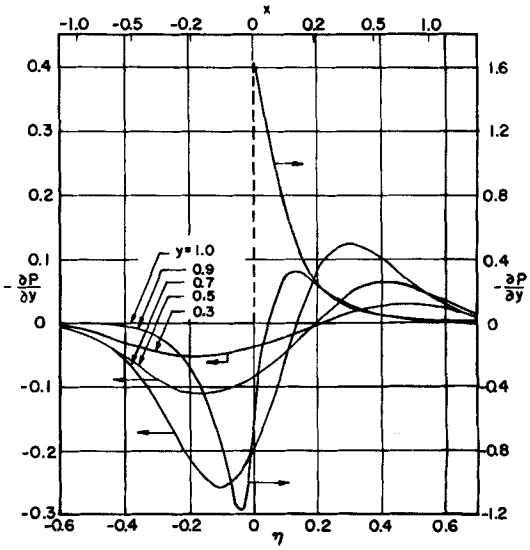

Fig. 7. $\partial P/\partial y$ as function of η, case II.

TABLE 4. EXCESS PRESSURE DROP*

η	Schlichting	Case I			Case II		
		$y = 0.9$	$y = 0.5$	$y = 0.1$	$y = 0.9$	$y = 0.5$	$y = 0.1$
0	0	0	0	0	−0.0563	0.0463	0.0628
0.05	0.033	0.0489	0.0260	0.0190	0.0102	0.0533	0.0671
0.15	0.072	0.1579	0.0660	0.0449	0.1134	0.0715	0.0778
0.25	0.100	0.1844	0.1075	0.0771	0.1582	0.0955	0.0929
0.35	0.127	0.1684	0.1484	0.1157	0.1746	0.1234	0.1135
0.45	0.153	0.1514	0.1834	0.1588	0.1843	0.1524	0.1402
0.55	0.176	0.1447	0.2118	0.2021	0.1957	0.1818	0.1730
0.65	0.196	0.1504	0.2379	0.2417	0.2124	0.2127	0.2108
0.75	0.217	0.1697	0.2686	0.2822	0.2380	0.2485	0.2557
0.85	0.248	0.2042	0.3109	0.3336	0.2772	0.2953	0.3124
0.95	0.301†	0.2775	0.3904	0.3937	0.3549	0.3793	0.3756

* Defined as $P(-\infty) - P(x) - 0.04x$.
† Schlichting shows this value for $x \to \infty$ also. Bodoia and Osterle (3) and Collins and Schowalter (4) show 0.338 as the asymptotic value and later (5) give 0.37.

flected in the lower values shown in Table 3. This reversal is apparently a result of the boundary condition at $x = 0$ which requires a sudden deceleration of the fluid. Case II exhibits only a small amount of difference at $\eta = 0.95$, and the accuracy of the solution can probably be judged by this fact. $\partial P/\partial y$ is not negligible at smaller η, and values of the excess pressure drop at different y's are not expected to be the same.

CONCLUSIONS

Numerical solutions which are exact in the sense that no terms in the governing differential equations have been neglected have been obtained for the entrance flow between parallel plates. Two types of upstream conditions were studied, namely a flat velocity distribution at the entrance (case I) and a flat distribution at a large distance upstream (case II). The latter case has more physical significance than the former, and very definite effects are transmitted upstream from the leading edges of the plates at a Reynolds number of 300, verifying that the usual boundary-layer assumption that $\partial^2 u_x/\partial x^2$ is negligible is not appropriate near the entrance.

It was found that the overall pressure drop and the inlet length predicted by boundary-layer theory methods are in reasonable agreement with those found for case II. It is probable that compensating errors are caused by the several assumptions made in the boundary-layer theory solution. However if velocity distributions and pressure gradients near the entrance are wanted, boundary-layer theory is not appropriate and the full differential equations must be solved with realistic boundary conditions.

The appearance of concavity and the associated points of inflection in the calculated velocity distributions is interesting, since according to Rayleigh (10) this would be expected to be associated with instability. It would be of interest to determine whether this concavity increases with increasing Reynolds number and whether it could be used to predict the transition to turbulent flow for case II.

The use of a transformation to reduce the infinite region to a finite region was successful, as was the use of Allen's device to obtain convergence. Use of relaxation factors varied in an empirical manner was useful in accelerating convergence.

NOTATION

A = function definede in Equation (A3)
a = $\Delta\eta$
B = function defined in Equation (A4)
b = Δy
C_i = coefficients defined in Equation (A9)
c = parameter in η transformation, Equation (14)
d = differential operator
$\exp(\ ) = e^{(\ )}$
G = constant
H = constant
h = elevation, ft.
M_ψ = relaxation factor for ψ
M_ω = relaxation factor for ω
P = dimensionless pressure, $(P' + \sigma h)\rho U^2$
N_{Re} = Reynolds number $4y_oU/\nu$
U = free stream and average velocity, ft./sec.
u_x = dimensionless x component of velocity u'_x/U
u_y = dimensionless y component of velocity u'_y/U
x, y, z = dimensionless cartesian coordinates x'/y_o, y'/y_o, z'/y_o
y_o = one half the spacing between parallel plates, ft.

Greek Letters

Δ = increment in
∂ = partial differential operator
η = function of x defined in Equation (14)
κ = function defined in Equation (A3)
λ = function defined in Equation (A4)
ν = kinematic viscosity, sq. ft./sec.
ρ = density, (lb.)(sec.^{2})/ft.^{4}
σ = specific weight, lb./cu. ft.
ψ = dimensionless stream function
ω = dimensionless vorticity
∇^2 = dimensionless Laplacian operator
∇^4 = dimensionless biharmonic operator

Subscripts

A,B,C,D,E,F,G,H,I = value at point A, B, C, D, E, F, G, H, I, Figure A1

Superscripts

(k) = kth iteration
Prime= on P, x, y, z, u_x, u_y, dimensional quantities

LITERATURE CITED

1. Schlichting, H., *ZAMM*, **14**, 368 (1934).
2. ———. "Boundary Layer Theory," 4 ed., p. 168, McGraw-Hill, New York (1960).
3. Bodoia, J. R., and J. F. Osterle, *Appl. Sci. Res.*, **A10**, 265 (1961).
4. Collins, Morton, and W. R. Schowalter, *Phys. of Fluids*, **5**, 1122 (1962).
5. ———, *A.I.Ch.E. Journal*, **9**, 98 (1963).
6. Allen, D. N. de G., and R. V. Southwell, *Quart. J. Mech. and Appl. Math.*, 8, Part 2, p. 129 (1955).
7. Forsythe, G. E., and W. R. Wasow, "Finite Difference Methods for Partial Differential Equations," Wiley, New York (1960).
8. Wang, Yui L., Ph.D. thesis, Part 2, Calif. Inst. Technol., Pasadena, California (1963).

9. ———, and P. A. Longwell, Tabular material has been deposited as document 7846 with the American Documentation Institute, Photoduplication Service, Library of Congress, Washington 25, D.C., and may be obtained for $2.50 for photoprints or $1.75 for 35-mm. microfilm.
10. Rayleigh, Lord, *Sci. Papers*, **1**, 474 (1880); **3**, 17 (1887); **4**, 197 (1913).

Manuscript received May 2, 1963; revision received August 12, 1963; paper accepted August 14, 1963.

APPENDIX

Preliminary Attempts at Solution

Several numerical methods of solution were tried in order to find one with which the iterations converged to a solution and which was reasonably efficient in its use of machine time. All were tried on case I, and in all schemes the partial difference equation written for a particular node was solved for the unknown at that node.

Initial work on Equation (11) with a coarse grid indicated that a single step iteration, that is one always using the latest values available, converged faster than did total step methods, which use the same set of values without replacement to calculate a complete new set. It also appeared that use of backward differences on first and third derivatives gave convergence, while central difference representations of these derivatives led to divergence.

A computer program was then written for Equation (11) with a 150 by 10 grid in terms of x and y. A parabolic velocity distribution was taken at $x = 24$. Backward differences were used for odd derivatives and central differences for even derivatives. It was found that the solution converged at a Reynolds number of 30 and diverged at 300.

Next Equation (11) was transformed to use η and y as independent variables, and a 10 by 10 grid was used. Again backward differences were used for odd derivatives, and central differences were used for even derivatives. The solution was found to converge for a Reynolds number of 60 and to diverge for 100 and higher Reynolds numbers. Thus the use of η did not appear to aid stability, but it did allow a significant reduction in the number of grid points without a penalty in accuracy.

Finally an adaption of the method described by Allen (*6*) was tried on a 10 by 10 grid in terms of η and y. The finite difference equations used are derived in this Appendix as Equations (A8) and (A16). Convergence was found for Reynolds numbers of 60, 100, 300, and 1,000. These calculations were not iterated sufficiently to obtain fully converged solutions however, and velocities were not calculated.

In order to speed up convergence the method of successive relaxation, described in connection with Equations (A17) through (A19), was tried on the 10 by 10 grid with Allen's method. Starting with a solution for a Reynolds number of 300 which was converged to the extent that the maximum percentage change in ψ was 0.001% for one iteration, convergence of ψ to 8 significant figures took sixty-seven iterations without use of relaxation factors (corresponding to M_ω and M_ψ each equal to 1) and similar convergence was obtained in fourteen iterations when successive relaxation was suitably employed. It was found that suitable starting values of the relaxation factors were about 1.5, that these should be decreased as the iterative process progressed, and that the best final values were usually less than unity. Several runs were made during which the relaxation factors were held constant, and in these cases either oscillation or divergence was observed. Although the manner in which these factors should be manipulated was not fully understood, it was found desirable to decrease M_ω faster than M_ψ.

Derivation of Finite Difference Equations

The method used to obtain a finite difference form for Equation (15) which gave convergence is due to Allen (*6*) and is as follows. Equation (15) can be rearranged to give

$$\left[\frac{\partial^2\omega}{\partial y^2} + \left(\frac{N_{Re}}{4}\frac{d\eta}{dx}\frac{\partial\psi}{\partial\eta}\right)\frac{\partial\omega}{\partial y}\right] + \left(\frac{d\eta}{dx}\right)^2 \left[\frac{\partial^2\omega}{\partial\eta^2} + \frac{\left(\frac{\partial^2\eta}{dx^2} - \frac{N_{Re}}{4}\frac{d\eta}{dx}\frac{\partial\psi}{\partial y}\right)}{\left(\frac{d\eta}{dx}\right)^2}\frac{\partial\omega}{\partial\eta}\right] = 0 \quad \text{(A1)}$$

or

$$A + \left(\frac{d\eta}{dx}\right)^2 B = 0 \quad \text{(A2)}$$

where

$$A = \frac{\partial^2\omega}{\partial y^2} + \left(\frac{N_{Re}}{4}\frac{d\eta}{dx}\frac{\partial\omega}{\partial\eta}\right)\frac{\partial\omega}{\partial y} = \frac{\partial^2\omega}{\partial y^2} + \kappa\frac{\partial\omega}{\partial y} \quad \text{(A3)}$$

and

$$B = \frac{\partial^2\omega}{\partial\eta^2} + \frac{\left(\frac{d^2\eta}{dx^2} - \frac{N_{Re}}{4}\frac{d\eta}{dx}\frac{\partial\psi}{\partial y}\right)}{\left(\frac{d\eta}{dx}\right)^2}\frac{\partial\omega}{\partial\eta} = \frac{\partial^2\omega}{\partial\eta^2} + \lambda\frac{\partial\omega}{\partial\eta} \quad \text{(A4)}$$

If A and κ are assumed constant in Equation (A3), the solution is

$$\kappa\omega = Ay + G + H\exp(-\kappa y) \quad \text{(A5)}$$

With reference to Figure A1 Equation (A5) was written for points B, D, and E and the resulting three equations solved to give an expression for A, taken to apply at point E:

$$A_E = \frac{\kappa_E[(\omega_B - \omega_E)\exp(\kappa_E b) - (\omega_E - \omega_D)]}{b[\exp(\kappa_E b) - 1]} \quad \text{(A6)}$$

Similarly, by assuming B and λ constant in Equation (A4), there is obtained

$$B_E = \frac{\lambda_E[(\omega_A - \omega_E)\exp(\lambda_E a) - (\omega_E - \omega_C)]}{a[\exp(\lambda_E a) - 1]} \quad \text{(A7)}$$

Equations (A6 and (A7) are substituted in Equation (A2) and solved for ω_E, giving

$$C_E\omega_E = C_A\omega_A + C_B\omega_B + C_C\omega_C + C_D\omega_D \quad \text{(A8)}$$

in which

$$C_A = \left(\frac{d\eta}{dx}\right)^2_E \lambda_E \exp(\lambda_E a)/a[\exp(\lambda_E a) - 1]$$

$$C_B = \kappa_E \exp(\kappa_E b)/b[\exp(\kappa_E b) - 1]$$

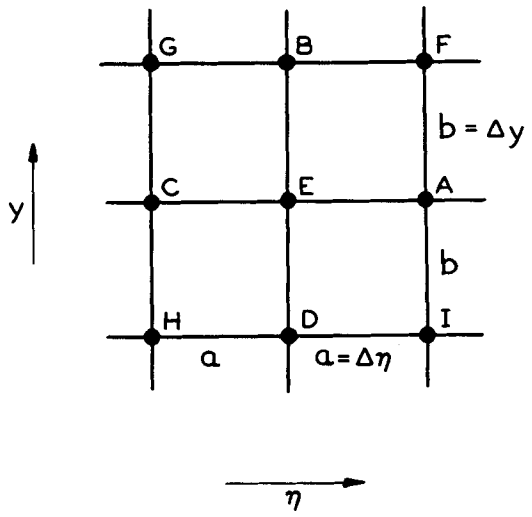

Fig. A1. Pattern of points.

$$C_C = \left(\frac{d\eta}{dx}\right)_E^2 \lambda_E/a\,[\exp(\lambda_E a) - 1] \quad \text{(A9)}$$

$$C_D = \kappa_E/b\,[\exp(\kappa_E b) - 1]$$

$$C_E = C_A + C_B + C_C + C_D$$

κ and λ were evaluated with central difference formulas to approximate the partial derivatives of ψ in Equations (A3) and (A4):

$$\kappa_E = \frac{N_{Re}}{8a}\left(\frac{d\eta}{dx}\right)_E (\psi_A - \psi_C)$$

$$\lambda_E = \left[\left(\frac{d^2\eta}{dx^2}\right)_E - \frac{N_{Re}}{8b}\left(\frac{d\eta}{dx}\right)_E (\psi_B - \psi_D)\right] \Big/ \left(\frac{d\eta}{dx}\right)_E^2 \quad \text{(A10)}$$

Differentiation of Equation (14) gives

$$\left(\frac{d\eta}{dx}\right)_E = c(1-\eta_E)^2 \quad \text{(A11)}$$

$$\left(\frac{d^2\eta}{dx^2}\right)_E = -2c^2(1-\eta_E)^3 \quad \text{(A12)}$$

The finite difference form used for Equation (15) is therefore Equation (A8), with the multipliers C_i defined by Equations (A9) through (A12), and is used to calculate ω_E.

The boundary conditions used with Equation (A8) are found in Equations (18) through (23) plus one derived from Equation (17) as

$$\omega_E = 2(1-\psi_D)/b^2 \text{ at } y_E = 1 \quad \text{(A13)}$$

As a matter of interest Equation (A3) can be equated to Equation (A6) written in an equivalent form, and the finite difference forms of the derivatives can be identified:

$$A_E = \kappa_E\left(\frac{\partial\omega}{\partial y}\right)_E + \left(\frac{\partial^2\omega}{\partial y^2}\right)_E = \kappa_E\frac{(\omega_B - \omega_E)}{b} + \frac{\kappa_E(\omega_B + \omega_D - 2\omega_E)}{b[\exp(\kappa_E b) - 1]} \quad \text{(A14)}$$

It is seen that a forward difference form is used for the first derivative. If the exponential term in Equation (A14) is expanded in power series, there is obtained

$$\left(\frac{\partial^2\omega}{\partial y^2}\right)_E = \frac{1}{b^2}\frac{\omega_B + \omega_D - 2\omega_E}{1 + \kappa_E b/2! + (\kappa_E b)^2/3! + \ldots} \quad \text{(A15)}$$

which approaches a conventional central difference representation as the grid spacing b approaches zero. Equation (A7) can be treated similarly.

Equation (16) is linear and was expressed in finite difference form by using conventional central differences as

$$2\left(\left[\frac{d\eta}{dx}\right) + \left(\frac{a}{b}\right)^2\right]\psi_E = a^2\omega_E + \left(\frac{a}{b}\right)^2(\psi_B + \Psi_D) + \left(\frac{d\eta}{dx}\right)^2(\psi_A + \psi_C) - a\frac{d^2\eta}{dx^2}(\psi_A - \psi_C) \quad \text{(A16)}$$

Equation (A16) is used to calculate ψ_E.

The transformation η as defined in Equation (14) is discontinuous at the origin, and the equations involving η cannot be applied at $\eta = 0$. However symmetry allows use of finite difference equations in terms of x and y at this line, which can be written from Equations (A8) through (A10) and (A16) by substituting $d\eta/dx = 1$, $d^2\eta/dx^2 = 0$, and $a = \Delta x$.

The rate of convergence of the iterative solution of elliptic difference equations can be markedly increased by a successive relaxation technique (7) which involves the use of a relaxation parameter in combination with the method of successive displacements (single step). When one uses the iteration for ψ as an example, the use of a relaxation parameter means determination of the new value of ψ_E, $\psi_E^{(k+1)}$ by the formula

$$\psi_E^{(k+1)} = \psi_E^{(k)} + M_\psi^{(k)}(\psi_E^{(k+1/2)} - \psi_E^{(k)}) \quad \text{(A17)}$$

in which $\psi_E^{(k)}$ is the present value, $\psi_E^{(k+1/2)}$ is the value of ψ_E calculated from Equation (A16), and $M\psi^{(k)}$ is the relaxation factor with

$$0 < M_\psi^{(k)} < 2 \quad \text{(A18)}$$

For linear difference equations which result in symmetric matrices with diagonal elements greater than zero and nondiagonal elements less than or equal to zero, it is found (7) that the optimum relaxation factor lies beween 1 and 2. However Equations (A8) and (A16) do not meet these requirements, and relaxation factors less than 1 were found useful.

New values of ω are found by use of the equation

$$\omega_E^{(k+1)} = \omega_E^{(k)} + M_\omega^{(k)}(\omega_E^{(k+1/2)} - \omega_E^{(k)}) \quad \text{(A19)}$$

in which $\omega_E^{(k+1/2)}$ is the value of ω_E calculated from Equation (A8).

Successive relaxation was used in the following manner for ψ. Calculations started at the point next to $\eta = 0$ and next to $y = 1$ and went down the column at constant η, then started at the top of the next column and went down, and so forth, until the point at the bottom of the column next to $\eta = 1$ was reached. At each point the existing values of ω and the latest values of ψ were used, and the result from Equation (A17) was stored as a latest value.

The method of successive relaxation used for ω was similar to that for ψ. Existing values of ψ and latest values of ω, from Equation (A19), were used.

After the solution has been determined in terms of ψ and ω, the velocities and pressures can be determined. With central differences and the $\eta - y$ grid used, point velocities are given by

$$(u_x)_E = \left(\frac{\partial\psi}{\partial y}\right)_E = \frac{1}{2b}(\psi_B - \psi_D) \quad \text{(A20)}$$

$$(u_y)_E = -\left(\frac{d\eta}{dx}\right)_E\left(\frac{\partial\psi}{\partial\eta}\right)_E = \left(\frac{d\eta}{dx}\right)_E\frac{1}{2a}(\psi_C - \psi_A) \quad \text{(A21)}$$

Equation (2) can be expressed as

$$-\frac{\partial P}{\partial x} = \left(\frac{d\eta}{dx}\right)\left(\frac{\partial\psi}{\partial y}\frac{\partial^2\psi}{\partial\eta\partial y} - \frac{\partial\psi}{\partial\eta}\frac{\partial^2\psi}{\partial y^2}\right) + \frac{4}{N_{Re}}\frac{\partial\omega}{\partial y} \quad \text{(A22)}$$

which was used in finite difference form as

$$-\left(\frac{\partial P}{\partial x}\right)_E = \left(\frac{d\eta}{dx}\right)_E\frac{1}{8ab^2}\Big[(\psi_B - \psi_D)(\psi_F - \psi_G + \psi_H - \psi_I) - 4(\psi_A - \psi_C)(\psi_B + \psi_D - 2\psi_E)\Big] + \frac{4}{bN_{Re}}(\omega_B - \omega_E) \quad \text{(A23)}$$

Central differences were used on ψ; however a forward difference was used on the term $\partial\omega/\partial y$ in accordance with the representation in Equation (A14).

Similarly use of Equation (3) leads to

$$-\left(\frac{\partial P}{\partial y}\right)_E = \left(\frac{d\eta}{dx}\right)_E^2\frac{1}{8a^2b}[(\psi_A - \psi_C)(\psi_F - \psi_G + \psi_H - \psi_I) - 4(\psi_B - \psi_D)(\psi_A + \psi_C - 2\psi_E)] - \left(\frac{d^2\eta}{dx^2}\right)_E\frac{1}{4ab}(\psi_B - \psi_D)(\psi_A - \psi_C) - \frac{4}{aN_{Re}}\left(\frac{d\eta}{dx}\right)_E(\omega_A - \omega_E) \quad \text{(A24)}$$

At $\eta = 0$ it was necessary to use equations in terms of an $x - y$ grid. These can be obtained from Equations (A20), (A21), (A23), and (A24) by taking $d\eta/dx = 1$, $d^2\eta/dx^2 = 0$, and $a = \Delta x$.